Current Advances in Cancer Science
Volume 1
Article ID: 100002

Research Article

Linkage Between Stemness and Epithelial–Mesenchymal Transition of Breast Cancer Cells Incubated on Viscoelastic Gel Substrates

Rie Sasaki[1], Ryohei Ohta[1] and Masami Okamoto[1]*

[1]Advanced Polymeric Nanostructured Materials Engineering, Graduate School of Engineering, Toyota Technological Institute, Japan

***Corresponding author**: Prof. Masami Okamoto, Advanced Polymeric Nanostructured Materials Engineering, Graduate School of Engineering, Toyota Technological Institute, 2-12-1 Hisakata, Tempaku, Nagoya 468 8511, Japan; E-mail: okamoto@toyota-ti.ac.jp

Received: January 05, 2022; **Accepted**: February 19, 2022; **Published**: February 26, 2022

Abstract

Aim: This study aimed to examine the effect of viscoelasticity of the substrate on the direct relation among cancer stemness, cellular motility and mesenchymal properties with induction of epithelial–mesenchymal transition (EMT) in both normoxia and hypoxia. **Methods:** Acrylamide copolymer-based gel substrates with different viscoelasticity were employed to evaluate the viscoelasticity effect on the direct relation among cancer stemness, cellular motility and mesenchymal properties with induction of EMT of human breast adenocarcinoma (MCF-7) cells in both normoxia and hypoxia. **Results:** Cellular migration speed (S) of MCF-7 cells was significantly upregulated with decreasing in coefficient of damping (tanδ). The softer gel substrate produced a large amount of surface molecule of cancer stem cells (CSC) marker CD44. In contrast, for the stem cell biomarker CD133 expression, their tanδ-dependent manner was not contributed by EMT phenomenon and was an independent from acquisition of the EMT. **Conclusion:** The substrate damping as potential physical parameter emerged the important linkage to cellular motility, cancer stemness, and EMT induction.

Keywords: *viscoelastic gel substrates, cancer cells, epithelial-mesenchymal transition, cancer stem cells, cellular motility*

Introduction

Cancer is ranked as leading cause of death in Japan. It is estimated that 50% of the population suffer from cancer in their lifetime. In 2019, about 30% of deaths are due to cancer, which is a major health problem [1]. Cancer morbidity and mortality in Japan are increasing year by year, with more than 360,000 new deaths each year due to the aging and longevity of the population [2].

Breast cancer is one of the most common malignancies in women and has the highest incidence and mortality among all female malignancies in Japan [1,3]. An average 5-year overall survival rate for breast cancer has been reported to be approximately 55% due to poor treatment outcomes for metastatic disease in resistance to radiation and chemotherapy [4]. Breast cancer treatment with a poor prognosis encourages research into effective cancer treatments. In short, breakthroughs in effective cancer treatment are essential.

Recently proposed hypotheses suggested that cancer stem cells (CSCs) and epithelial-mesenchymal transition (EMT) play crucial roles in cancer metastasis, recurrence, and drug resistance [5]. CSCs were first proposed by Virchow and Conheim. Subpopulations of cancer cells resemble the same properties as embryonic cells, such as their ability to proliferate, and cancer derives from the activation of dormant cells in the same tissue. Some CSCs self-replicate and produce many heterogeneous, highly proliferative cancer cells to form primary tumors [6].

EMT causes morphological and functional changes in epithelial cells, resulting in the acquisition of mesenchymal-like features by cancer cells. The epithelial program causes epithelial cells to lose cell-cell and extracellular matrix

(ECM) interactions and undergo cytoskeletal reorganization and to acquire the morphological and functional characteristics of mesenchymal cells. The tumor microenvironment can induce EMT. The ability of metastatic cancer to shift the mode of motility by EMT is one of the main features of invasion. Understanding the interaction of the microenvironment with cancer cells is also important for advances in cancer treatment [7,8].

Most proliferative cancer cells are killed by chemoradiotherapy. However, like sarcomas, CSCs undergoing EMT that characterize the mesenchymal system are resistant to anticancer therapy. Therefore, the CSC survives and causes a recurrence of the cancer. Recent studies have shown that EMT inducers not only induce EMT, but also enhance the CSC function of cancer cells [9].

Targeting the CSCs and EMT populations can lead to breakthroughs in cancer treatment. The relationship between CSCs and EMT has received considerable attention. The introduction of EMT is believed to facilitate CSC functionality. However, there is no detailed analysis of the role of EMT in the regulation of breast cancer cell stem cell characteristics.

To solve this profound problem, we need an artificial ECM with various viscoelastic properties that mimics the microenvironment *in vivo*. This study examines the effect of substrate viscoelasticity on the direct relationship between cancer stemness, cell motility, and mesenchymal properties with EMT induction in both normal and hypoxic conditions.

Materials and Methods

Preparation of acrylamide copolymer gels

Acrylamide (AAm, Sigma-Aldrich), *N*-acryloyl-6-aminocaproicacid (ACA, Santa Cruz), *N,N'*-Methylenebisacrylamide (BIS, Sigma-Aldrich), ammonium persulfate (APS, Sigma-Aldrich), and *N,N,N',N'*-tetramethylethylendiamine (TEMED, Sigma-Aldrich), were used without further purification. Millipore Milli Q ultrapure (specific resistance: 18 MΩcm, total organic carbon (TOC) <20 ppb, Merck Millipore Japan Co.) water through dialysis membrane was used in all experiment.

After polymerization, the AAm-ACA copolymer (AC) gels were fully hydrated (swelling) in phosphate-buffer saline (PBS, Nacalai Tesque, Kyoto) and washed with 0.1 M of 2-(*N*-morpholino) ethanesulfonic acid buffer (MES, Dojindo) with 0.5 M NaCl (Sigma-Aldrich) at pH 6.1. The viscoelastic properties of AC gels were controlled with varying amount of cross-linker BIS solution (2 wt% in Milli Q water) and Milli Q water (Supplementary Table 1). The details of preparation [10] and rheological characterization [11] were described in previous papers.

Immobilization of collagen on AC gels

For conjugation of type-I collagen on the AC gel surface, the solution of 0.2 M of 1-ethyl-3-(3-dimethyl aminopropyl) carbodiimide hydrochloride (EDAC, Tokyo Chemical Industry Co., Ltd., Japan (TCI)) and 0.5 M of N-hydroxysuccinimide (NHS, TCI) was prepared in MES buffer and then dehydration condensation reaction was performed for 30 min at ambient temperature. The gels modified with EDAC were washed with cold 40% methanol diluted with PBS and subsequently reacted with type-I collagen (Cellmatrix I-C, Nitta Gelatin, Inc.) for overnight at 4°C in HEPES (2-[4-(2-hydroxyethyl)piperazin- 1-yl]ethane-sulfonic acid, Gibco, Life Technology) buffered saline solution (2 × HBS: NaCl, 280 mM: Na_2HPO_4, 1.5 mM: HEPES, 50 mM) to adjust at pH 9.0. Then AC gels modified with type-I collagen were sterilized with germicidal UV light for 30 min. Finally, all AC gels were equilibrated in high glucose Dulbecco's modified Eagle's medium (DMEM) (Nacalai Tesque, Kyoto) supplemented with 10 % (v/v) FBS at 4°C for overnight. Jiang et al. reported the resulting nanostructured collagen matrix was about 3 nm in thickness [12]. For comparison, type-I collagen coated plates (TCP-coat) were prepared by adding Cellmatrix I-C solution onto 24-well tissue culture plates (TCP) and heated at 37°C for 2 h. Then added solution was removed. The details of preparation were described in our previous papers [11].

Cell culture

Human breast adenocarcinoma cell line, MCF-7 (ATCC) were cultured in high glucose Dulbecco's modified Eagle's medium (DMEM) (Nacalai Tesque, Japan) supplemented with 10% (v/v) FBS, 100 unit/mL penicillin (Nacalai Tesque, Kyoto), and 100 μg/mL streptomycin (Nacalai Tesque, Kyoto), grown at 37°C under 5% CO_2 atmosphere and 95% relative humidity (normoxia) or hypoxic condition (94% N_2, 5% CO_2, and 1% O_2) at 37°C. Cells were grown to 70-80% confluence at normal culture condition before being seeded onto the gel substrates.

Immunofluorescence staining

MCF-7 cells were seeded at the density of 1.0×10^4 cells cm^{-2} on AC gels modified with type-I collagen substrates (AC-soft, AC-mid, and AC-stiff) and type-I collagen coated 24-well TCP under normoxic or hypoxic conditions for a period of 3 days. The cells were fixed with 4% paraform aldehyde for 15 min at room temperature. The cells were then washed with phosphate-buffer saline (PBS, Nacalai Tesque) and permeabilized with 0.1% Triton X (Nacalai Tesque) for 6 min. The fixed cells were washed twice with PBS and blocked with 2% bovine serum albumin (BSA, Wako) in PBS for 60 min. The cell cytoskeleton and nuclei were stained by Alexa-Fluor 488 phalloidin (Life Technologies) and Hoechst 33342 (Life Technologies) for 20 min. All stained samples were imaged using a fluorescent microscope (EVOS FL Auto, Life Technologies).

The cellular morphologies (nuclear elongation factor, cytoplasm roundness, and nuclear area (AN) to cytoplasm area (AC) ratio (A_N/A_C)) were manually quantified by following the contour of each cell (n=32). The nuclear elongation factor, cytoplasm roundness, and A_N/A_C were calculated as the major axis/minor axis of the nucleus, 4(area)/(π(major axis)^2) of the cytoplasm, and area of nuclear (AN)/area of the cytoplasm (AC), respectively. By definition, the cytoplasm roundness is equal to 1 for a completely round cell.

Real time polymerase chain reaction (RT-PCR)

The total RNA was extracted from the cells cultured for three days using Fast Gene™ RNA Premium Kit (Nippon genetics). Then the RNA was subjected to reverse transcription using a Transcriptor Universal cDNA Master (Roche) following the manufacturer's instructions. The reaction solutions included 5 μL of KAPA SYBR® FAST qPCR Master Mix (KAPA BIOSYSTEMS), 200 nM forward and reverse predesigned primers [11], and 1/10 of cDNA template in a 10 μL volume. The resulting cDNA yield was then subjected to RT-PCR using Light Cycler® 96 system (Roche). The results were analyzed with Light Cycler® 96 software (Roche). The cDNA samples were analyzed for expression of E-cadherin (CDH1), N-cadherin (CDH2), transforming growth factor beta (TGF-β), hypoxia-inducible factor 1α (HIF-1α) and vimentin, relative to the glyceraldehyde-3-phosphatase dehydrogenase (GAPDH) as an internal standard for sample normalization. In addition, the cDNA samples of day 7 were analyzed for expression of snail family zinc finger 2 (SNAI2) and zinc finger E-box binding homeobox 1 (ZEB1). The details of characterization were described in our previous paper [11].

Cellular migration

MCF-7 cells were seeded on the gel substrates and cultured under normoxic or hypoxic conditions. Both cells were seeded at the density of 5×10^3 cells cm^{-2} for 3 days, pre-cultured for 24 h to attach the cells to the substrates. An environment of 37°C temperature, normoxic or hypoxic condition was applied during the time-lapse measurement. The cells were stained with 0.1 μg mL^{-1} of Hoechst 33342 for 20 min prior to time-lapse experiment. The blue, fluorescent images of the tracers were obtained every 15 min for 16 hours by EVOS FL Auto fluorescent microscope (Life Technologies). To track the cell movement, the position of 20 individual centroids [$x(t)$, $y(t)$] of cell nucleus were obtained by a Mosaic particle tracker for ImageJ developed by Helmuth et al. [13]. The start points of each cell were defined at the same position.

Characterizing the cellular migration using the persistent random walk (PRW) model

The obtained x, y values were first transferred into mean squared displacement (MSD) as equation (1)

$$MSD(\tau) = \left[\langle \left(x(t+\tau) - x(t)\right)^2 + \left(y(t+\tau) - y(t)\right)^2 \rangle\right]_n$$

where x and y are position of cells, t is time, and τ is the time lag between positions of cells, n is the number of tracked cells, <...> indicates time average, and [...] indicates cell average. Calculated MSD was assessed by applying model reported by several researchers [14,15]. 2D MSD for PRW model can be expressed by equation (2)

$$MSD(\tau) = 2S^2P^2(e^{-\frac{\tau}{P}} + \frac{\tau}{P} - 1)$$

Where S is the cellular migration speed and P is the persistent time. Cellular diffusivity D is calculated as $D=S^2P/2$.

Flow cytometric analysis

A total of 1×10^6 cells seeded onto the gel substrates for 7 days were suspended in 100 µL PBS with 0.5% BSA. The mouse anti-human CD133 mAb (Alexa Fluor 488-conjugated, Cell Signaling Technology) and rat anti-human CD44 mAb (PerCP-Cy5.5-conjugated, Cell Signaling Technology) were appropriately diluted in the FcR blocking reagent to a final volume of 20 µL. The antibodies were added to the cells, and mixture was incubated on ice according to the manufacturer's procedures. The cells were washed and resuspended in a suitable amount of buffer for analysis by flow cytometer (Attune® NxT Acoustic Focusing Cytometer, Thermo Fisher Scientific). Propidium iodide (Sigma-Aldrich) staining was applied to exclude the dead cells. Data analysis was performed with FlowJo v.10.0 Software.

Statistics

All data presented are expressed as the mean and standard deviations (±SD). Statistical analysis was performed using one-way analysis of variance with Tukey-Kramer' *post-hoc* testing using Excel 2013 with Statcel4 v.2.0 Software (OMS Publishing Co., Tokyo, Japan), and significance was considered at a probability of $p<0.05$.

Results

Viscoelasticity of AC gels

The viscoelastic properties of the substrates (AC gel and TCP) are characterized by tanδ and storage modulus (G') (Figure 1). In general, for viscoelastic materials, hard and hard materials such as metal and ceramic show high rigidity and low loss. On the other hand, soft materials have higher damping and lower rigidity. The solid line is the viscoelasticity figure of merit (VFOM) $(G'/\rho) \times (\tan\delta)^{0.5}=10^5$ m^2s^{-2}, using ρ as the density, steel, aluminum, poly (methyl methacrylate) (PMMA), TCP (PS), and natural rubber. It was found in traditional solid materials [11,16]. When the tanδ value is 0.04 to 0.26, the VFOM value of AC gel (~10^{-2} m^2s^{-2}) is 7 orders of magnitude lower than the VFOM value of solid material. This is achieved by a soft matrix containing the crosslinker BIS molecule. Figure 1 shows the biomedical properties of the tissue in terms of stiffness (modulus). Compliant tissues such as the lungs show low stiffness (400 Pa), while tissues exposed to high mechanical loads such as bones and skeletal muscles show high stiffness with rigidity four orders of magnitude higher (104–106 Pa) [11,17].

Effect of viscoelasticity of AC gels on cellular morphology

Supplementary Figure 1 shows the cell morphology of MCF-7 cells cultured on different TCP substrates coated with AC gel and type I collagen (TCP coat) in both normal and low oxygen conditions on day 3. is showing. TCP without collagen coating on day 3 is shown. The corresponding morphological parameters (cytoplasmic roundness, A_N/A_C, and nuclear elongation factor) are summarized in Figure 2.

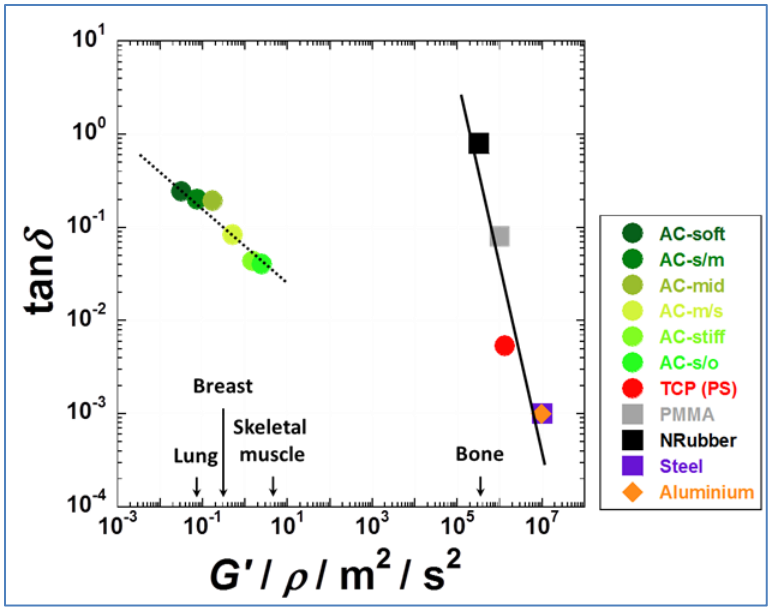

Figure 1. Damping coefficient (tanδ) and relative storage modulus (G′/ρ) map for AC gels and various conventional materials at 25°C. The solid line represents a viscoelastic figure of merit (VFOM) $(G'/\rho) \times (\tan\delta)^{0.5}=10^5$ m^2s^{-2}, for steel, aluminium, poly(methyl methacrylate) (PMMA), TCP (PS), and natural rubber [16]. The broken line represents VFOM for AC gels; $(G'/\rho) \times (\tan\delta)^{2.5}=10^{-2}$ m^2s^{-2}. The biomedical properties of a tissue in terms of stiffness (elastic modulus) are shown on the x-axis [17].

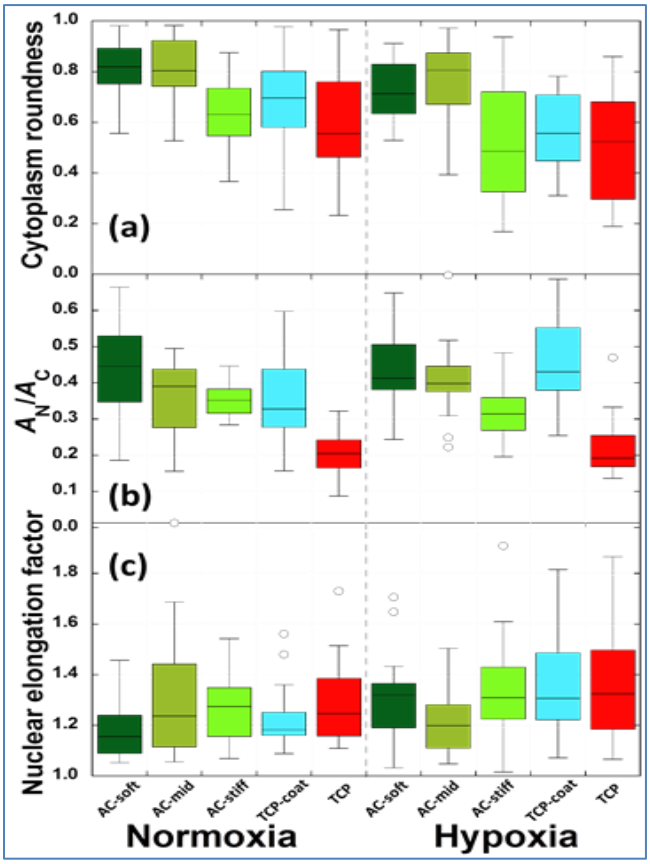

Figure 2. Quantification of the cellular morphologies of (a) cytoplasm roundness, (b) A_N/A_C ratio, and (c) nuclear elongation factor as boxplots for MCF-7 cells cultured on different substrates of AC gels, TCP-coat, and TCP under both normoxic and hypoxic conditions at day 3.

For MCF-7 cells cultured in both normal and hypoxic conditions, the cells spread with multicellular aggregates (colony forming). MCF-7 cells cultured on hard substrates (TCP coated, TCP, and AC hard) spread and have less circular morphology than other substrates (Figure 2a). The nuclear area-to-cytoplasmic area ratio (A_N/A_C) (Figure 2b) and the nuclear elongation factor (Figure 2c) represent the extent to which stress is transferred to the nucleus.

With this in mind, MCF-7 cells cultured on more stiffer substrates (TCP-coat and TCP) exhibit more spread and elongated morphologies due to much lower values in both A_N/A_C and cytoplasm roundness, and higher values in the nuclear elongation factor in comparison with those of MCF-7 cells incubated on AC-soft or AC-mid substrates. This phenomenon was similar to the results reported by several researchers [10,18]. That is, the cells could spread and attach to the stiff substrate rather than soft substrate.

Response to AC gel substrates, TCP-coat and TCP for incubation of MCF-7 cells does not exactly follow the same trend of the feature reported by previous papers [10,18]. This is presumably due to the colonization, which leads to an enhanced cell-cell contact via E-cadherin, following the less traction forces (contractility) generation and transmitted stresses to nucleus occurring [15].

The similar trend is observed in both normoxic and hypoxic conditions. As seen in Supplementary Figure 1 and Figure 2, the hypoxic treatment had no remarkable effect on MCF-7 cell's morphologies. This is supported through detail cellular migration analysis under both normoxic and hypoxic conditions at day 3.

Effect of substrate properties on motility of cells

Cellular motility

The representative recorded trajectories of MCF-7cells cultured on different substrates of AC gels, TCP-coat, and TCP under both normoxic and hypoxic conditions over 16 h at day 3 point are shown in Figure 3. For the cells on AC-soft (G' of 32 Pa) and AC-mid (G' of 174 Pa) substrates, their migrations are restricted compared to those on AC-stiff (G' of 1,510 Pa), TCP-coat, and TCP (G' of 1.4 GPa), while the cells migrated in random directions. As expected, increasing in stiffness of the substrates leads cells to move generally (Figure 3c) and farther away with higher motility (Figure 3d,3h) regardless any direction.

Another feature is that the cells cultured on TCP have some adverse effect on migration with a significant decrease in displacement than that on TCP-coat (Figure 3e). This trend is supported by the substrate surface that coated with type-I collagen. The same trend is observed under normoxic condition (Figure 3j).

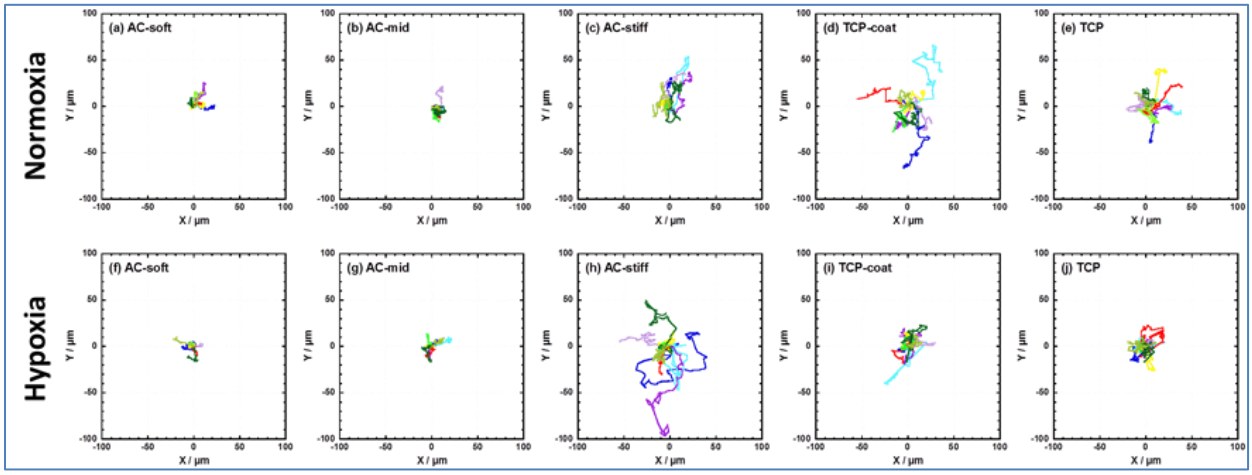

Figure 3. Representative trajectory of MCF-7 cells cultured on five different substrates under both normoxic (a-e) and hypoxic (f-j) conditions over 16 h at day 3. The data were obtained in 200 × 200 μm^2.

Cellular migration analysis by PRW model

To discuss the diffusion of the seeded cells on the substrates the calculated MSD values (Supplementary Figure 2) and characteristic parameters, cellular migration speed (*S*), persistent time (*P*), and cellular diffusivity (*D*) given by Eqn (2) are presented in Figure 4. MCF-7 cells cultured on AC-stiff substrate under hypoxia exhibit the highest value of S (0.60 μm/min) at day 3, while slight increasing in S under normoxic condition (0.67 μm/min) is observed on the same gel substrate. The *S* value of the cells on AC gel substrates under hypoxia changes obviously higher with increasing in gel stiffness (2.4-fold change between AC-stiff and AC-soft) accompanied by an enhancement in the vitality (*P*). The *D* value is the balance between *S* and *P*. AC-stiff substrate exhibits a one order of magnitude larger *D* value in comparison to AC-soft or AC-mid. Overall, *D* is significantly up-regulated under both oxygen concentration conditions and the cellular motility on AC-stiff substrate is enhanced. For MCF-7 cells in both normoxia and hypoxia, a slight motility reduction on TCP-coat of the cells reflects the suppression of *S* and *P*, following the decrease in *D*. In this regard, MCF-7 cells are rather less-invasive cancer cells presumably due to the multicellular aggregation (Figures 2a,2b).

The *D* value is important for understanding how quick the cancer cells can invade to vasculature system or lymph node. In general, metastatic cells can be distinguished from non-invasive cancer cells by reduced cytoskeletal stiffness (ratio of A_N and A_C: Figure 2b) and increased deformability (Figure 2a).

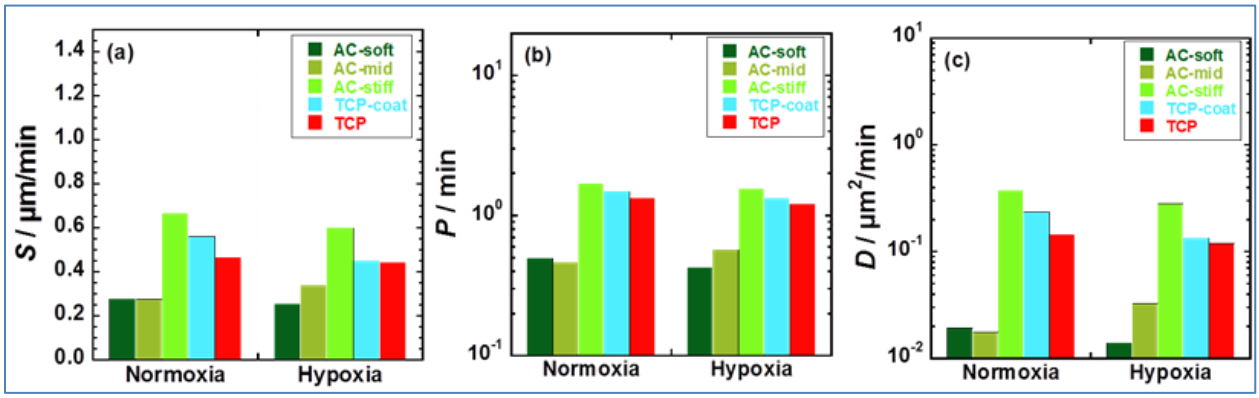

Figure 4. Summary of the cellular migration parameters calculated from MSD of MCF-7 cells in both normoxia and hypoxia: cellular migration speed (*S*) (a), persistent time (*P*) (b), and cellular diffusivity (*D*) (c) at day 3 cultured on five different substrates.

Linkage to substrate viscoelasticity and motility of cells in cellular morphologies

The cellular morphological parameters are chosen to clarify the relationship between morphology induced by physical properties of substrates and cellular motility. Cellular migration speed (*S*) is plotted as a function of morphological parameters of cytoplasm roundness, A_N/A_C, and nuclear elongation factor (Figure 5). For MCF-7 cells in both hypoxia and normoxia, linear relations between cellular deformability and migration speed are found on all substrates with different stiffness (except TCP). The *S* values are upregulated with increasing in deformability (cytoplasm roundness) (Figures 5a,5d) of the cells on the substrates. The effect of cytoskeletal stiffness (A_N/A_C) on cellular migration speed is plotted in Figures 5b,5e. The decreasing in cytoskeletal stiffness, which is equal to the increasing in cellular spreading factor, is also beneficial to understand the metastatic potential under both oxygen concentration conditions. However, for comparison with cytoplasm roundness, such robust correlation is not obtained in the morphological parameters of A_N/A_C. The plot of nuclear elongation factor versus S does not follow the same trend (Figure 5c).

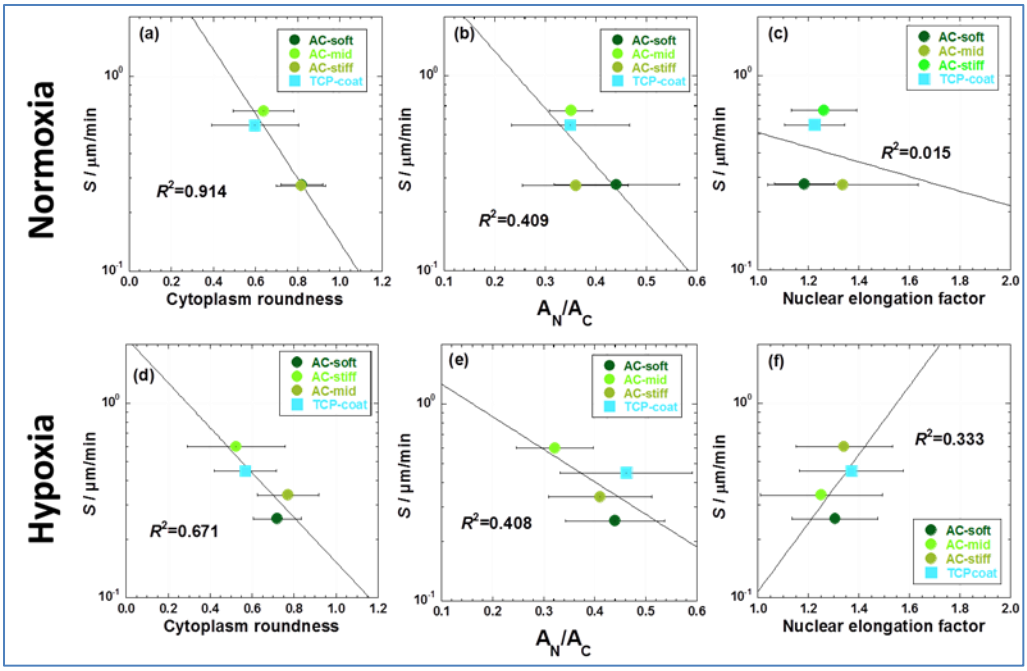

Figure 5. Relationships between cellular migration speed (*S*) and morphological parameters of cytoplasm roundness ((a) and (d)), A_N/A_C ((b) and (e)), and nuclear elongation factor ((c) and (f)) for MCF-7 cells at day 3 cultured on four different substrates under normoxic (a-c) and hypoxic (d-f) conditions. The solid line in each panel indicates semi-log linear regression.

Cellular migration speed (S) in MCF-7 cells under hypoxia is upregulated with decreasing in damping coefficient (tanδ) (Figures 6a,6d). Although the stiff substrate increased cellular motility, as discuss in above Section, our results found that the migration speed is not robustly correlated with substrate stiffness (relative storage modulus (G′/ρ): data not shown). This result suggests that the decreasing in damping is the driving force of the cellular migration in the cells. In addition, interestingly, the decreasing in tanδ promotes the persistent time (*P*) in a semi-log linear relation (Figures 6b,6e), while the results of the cellular diffusivity (*D*) have no robust correlation with tanδ (Figures 6c,6f).

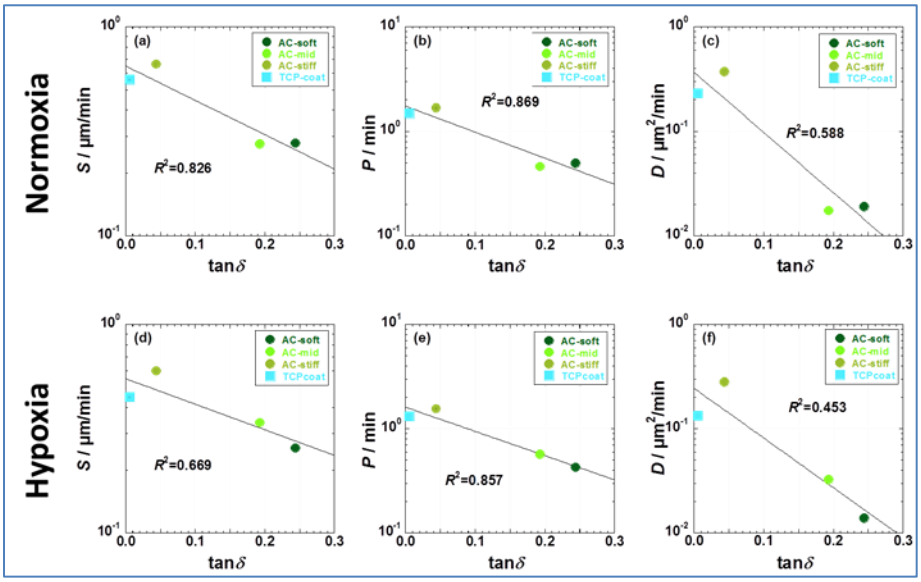

Figure 6. Relationships between cellular migration speed (*S*) ((a) and (d)), persistent time (*P*) ((b) and (e)), and cellular diffusivity (*D*) ((c) and (f)) against damping coefficient (tanδ) for MCF-7 cells at day 3 cultured on four different substrates under normoxic (a-c) and hypoxic (d-f) conditions. The solid line in each panel indicates semi-log linear regression.

Extensive studies have been made in a mechanotransduction via surface topography and stiffness on the substrates, in which the cells respond to applied forces and exert forces in the substrate (ECM) [19-22]. Such forces can change cell morphology and cytoskeletal structure due to the traction forces (contractility) generation, which influence cell response and cell fate. Essentially, the cells feel stiffness, however, tanδ value might be more favourable to understand the basic of cell-ECM interactions and mechanotransduction. For this reason, tanδ value has correlation to the morphological parameters of cytoplasm roundness (deformability) and nuclear elongation factor in the cells (Figures 7a,7d,7f).

The plots of cytoskeletal stiffness (A_N/A_C) versus tanδ do not follow the same trend (Figures 7b,7e), suggesting the colonization inhibits the cellular spreading, as mentioned above. The upregulation of deformability (Figures 7a,7d) and nuclear elongation factor (Figure 7f) are undergoing in less-invasive MCF-7 cells on the substrates. The damping coefficient is responsible for the cellular morphologies.

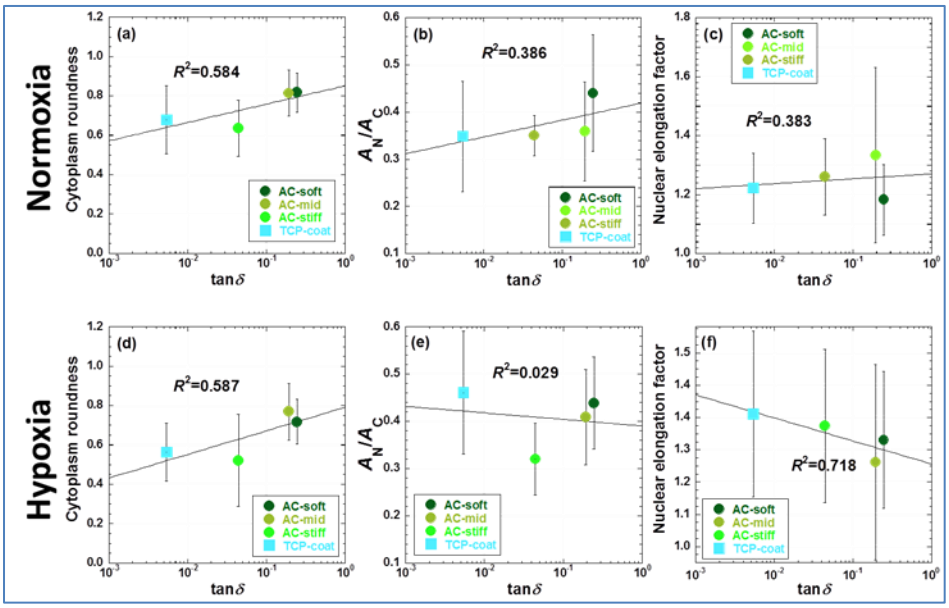

Figure 7. Relationships between morphological parameters of cytoplasm roundness ((a) and (d)), A_N/A_C ((b) and (e)), and nuclear elongation factor ((c) and (f)) and damping coefficient (tanδ) for MCF-7 cells at day 3 cultured on four different substrates under both normoxic (a-c) and hypoxic (d-f) conditions. The solid line in each panel indicates semi-log linear regression.

AC gel substrate contribution to CD133 and CD44 expression

A subpopulation of cancer cells, the CSCs, was found to display stem cell characteristics that influence tumorigenesis. These CSCs have various cancer-promoting characteristics such as self-renewal differentiation, chemoresistance, and metastatic potential [23,24]. CSCs express various CSC markers such as CD133, CD44, and CXCR4 [25]. The expression of CD133 is a strong predictor of declining prognosis, as high CD133 levels conversely relate to low 5-year overall survival and disease-free survival rate in cancer patients [26]. Another putative CSC marker is the cell-surface glycoprotein CD44, which was reported to be an adhesion molecule expressed in CSCs [27]. When upregulated, CD44 increases tumor growth and anti-apoptotic property [28]. Both CD133 and CD44 are well-recognized stem cell biomarkers express in breast cancer [29].

To delineate CD133 and CD44 expression in MCF-7 cells incubated on six different AC gel substrates and TCP-coat, we used flow cytometry to analyze the expression of these surface markers for CSCs after double-staining with anti-CD133-FITC and anti-CD44-PreCP antibodies. Supplementary Figure 3 shows a distribution of CD133 and CD44 expression with a $CD133^+CD44^-$ population of 1.46%, a $CD133^-CD44^+$ population of 0.81%, and a $CD133^+CD44^+$

population of 0.025% after the cells incubation on AC-soft substrate in hypoxia at day 7. The multiple-marker detection (co-expression) exhibits very low percentage of population in the cells.

For comparison, the expression levels at each substrate tested in this study are plotted as a function of tanδ (Figure 8). The $CD133^+CD44^-$ levels are markedly elevated with increasing in tanδ up to around 0.09 and have a decreasing trend for the cells cultured on AC-soft substrate under both oxygen concentration conditions (Figure 8a). Under normoxic and hypoxic conditions, the $CD133^-CD44^+$ levels are promoted by damping coefficient. The level of $CD133^-CD44^+$ is over 250-fold for the cells cultured on AC-soft substrate in comparison with that on AC-s/o in normoxia, suggesting that the softer gel substrate produce a large amount of surface molecule of CD44 (Figure 8b). From these findings, the expression of $CD133^-CD44^+$ is uncoupled from that of $CD133^+CD44^-$ in MCF-7 cells under different oxygen concentration levels.

For the co-expression of $CD133^+CD44^+$, more stem-like properties as compared with other population, seems to be affected by the combination of both $CD133^+CD44^-$ and $CD133^-CD44^+$, i.e., a further increase of the levels in the cells incubated on AC-soft (tanδ=0.244) via AC-mid (tanδ=0.193) substrate is observed (Figure 8c).

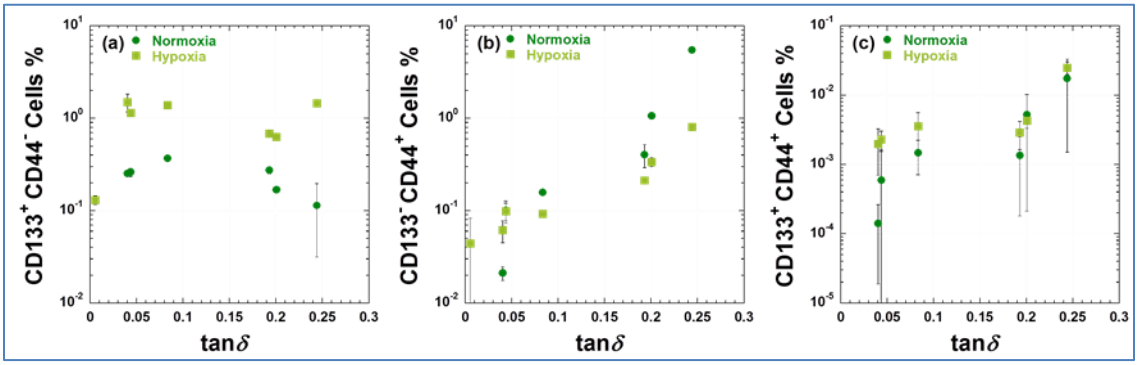

Figure 8. Relationships between $CD133^+CD44^-$(a), $CD133^-CD44^+$ (b), and $CD133^+CD44^+$ (c) expression and damping coefficient (tanδ) for MCF-7 cells at day 7 cultured on six different AC gel substrates and TCP-coat under both normoxic and hypoxic conditions.

AC gel substrate induced EMT

The gene expression changes are investigated to understand the role of ECM for malignant phonotype. In this study, typical epithelial cell marker of E-cadherin (CDH1) and mesenchymal marker of vimentin and CDH2 [30-34] were chosen because EMT is a critical phenomenon induces cancer metastasis [19-22,35-40].

To know detail of EMT and metastasis, transforming growth factor β (TGF-β) [30,41,42] and snail family zinc finger 2 (SNAI2) [30,43,44] and zinc finger E-box binding homeobox 1 (ZEB1) [41,43-46] were added to analysis. TGF-β is known to induce EMT. SNAI2 and ZEB1 are potent repressor of epithelial cell marker E-cadherin (CHD1) gene expression. Cancer cells respond to the hypoxic microenvironment through the activity of hypoxia inducible factor 1α (HIF-1α) [47-49] that behaves as a promotor of EMT.

Figure 9 shows the gene expression (HIF-1α, TGF-β, vimentin, CDH2, ZEB1, SNAI2, and CDH1) for MCF-7 cells cultured on AC gel substrates and TCP-coat (including TCP) at day 7 as a function of tanδ under both normaxic and hypoxic environment. In both normoxia and hypoxia, MCF-7 cells incubated on AC-soft (tanδ=0.244), and AC-mid (tanδ=0.195) substrates show a significant change in HIF-1α expression (Figure 9a). While significant repression is observed for the cells culture on AC-s/m (tanδ=0.201). For TGF-β level under hypoxic condition, similar change is obtained in MCF-7 cells on all AC gel substrates and TCP-coat (Figure 9b). The cells incubated in the normoxic group do not show a significant increase in TGF-β expression.

For vimentin expression, this surface protein is expressed with similar manner on AC gel substrates and TCP-coat (Figure 9c). The vimentin level under hypoxic condition is markedly increased in the cells incubated on AC-soft (720-

fold) and AC-mid (360-fold) in comparison with that of incubation from AC-stiff substrate up to TCP-coat. Similar result is obtained when the cells are incubated in normoxia, while the cells express less vimentin (30-fold) in comparison with AC-soft and AC-stiff substrates.

The expression of CDH2 shows in Figure 9d. For CDH2 expression, similar changes (440-fold in hypoxia) are obtained in the cells on AC gel substrates as compared with the results in vimentin expression (Figure 9c). For transcription factors (ZEB1 (Figure 9e) and SNAI2 Figure 9f)), more upregulation of ZEB1 and SNAI2 in the cells incubated on AC-soft and AC-mid substrates in hypoxia has shown a trend to further induce EMT. The behavior is consistent with the results obtained in TGF-β expression under both normoxic and hypoxic conditions.

As expected, the expression level of epithelial cell marker CHD1 associated with EMT is significantly lower than that observed in CDH2 expression level (Figure 9g), indicating that EMT is more promoted in both normoxic and hypoxic environment.

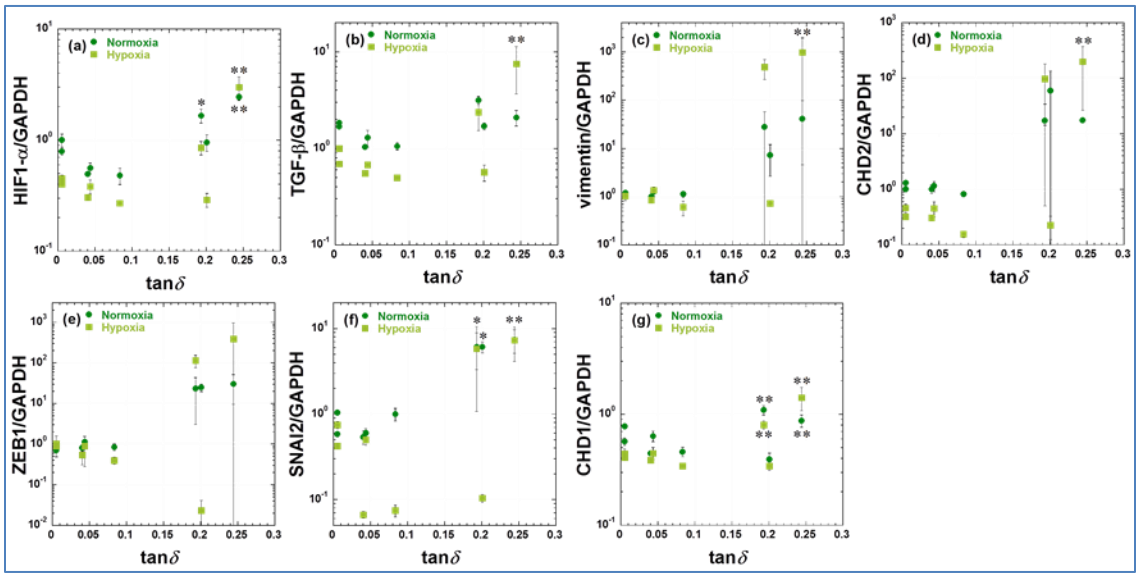

Figure 9. Effect of the substrate tanδ on gene expression of (a) HIF-1α, (b) TGF-β, (c) vimentin, (d) CDH2, (e) ZEB1 (f) SNAI2, and (g) CDH2 for MCF-7 cells after 7 days culture under both normoxia and hypoxia. (*p<0.05 and **p<0.01).

Taken together, these results indicate that AC-soft and AC-mid substrates cause significant change in induction (transcription factors (ZEB1 and SNAI2) associated with EMT) and acquisition (vimentin and CDH2 expressions) of the EMT. Up to now, we have limited information regarding viscoelastic gel substrate mediated EMT. The effect of tanδ feature from AC-soft (0.244) to AC-mid (0.195) including AC-s/m (0.201) on gene expression might explain by a further study.

Discussion

In each of gel substrates tested in this study, the effect of tanδ feature on the gene expression of vimentin and CDH2 is more beneficial for MCF-7 cells under different oxygen concentration levels, in which a significant level of upregulation is evident for the cells incubated on AC-soft substrate.

When we correlate expression of $CD133^{-}CD44^{+}$ with vimentin and/or CDH2 in MCF-7 cells, we observe a significant association between $CD133^{-}CD44^{+}$ level and vimentin/CDH2 expression in the cells incubated on AC-soft substrate. These results indicate that $CD133^{-}CD44^{+}$ level is involved in regulating the expression of HIF-1α. We assume that breast CSCs characterized $CD133^{-}CD44^{+}$ level may have a survival advantage under hypoxic condition, since EMT has been demonstrated to contribute to drug resistance in breast cancer [50,51].

So far, the induction of EMT is believed to promote CSC features. CSC theory has been widely accepted as a central principle to explain tumor aggressiveness, recurrence, chemoresistance and even metastasis through EMT phenomenon [9,50,52].

The role of CD44, a hyaluronic receptor, is to promote cell-adhesion and assembly of cell surface growth factors, especially in the maintenance of cell-matrix interactions and maintenance of a stem cell phenotype [53]. Mechanisms regarding how tanδ feature controls CD44 expression are obscure in terms of the regulation of a large variety of signaling pathways although main receptor CD44 is identified as main components of CSC niche.

We next examined the connection between $CD133^{+}CD44^{-}$ with vimentin and/or CDH2 in the cells. The results in Figure 8(a) indicate that $CD133^{+}CD44^{-}$ levels are not associated with vimentin/CDH2 expression. In the $CD133^{+}CD44^{-}$ levels, their tanδ-dependent manner is not contributed by EMT phenomenon and is an independent from acquisition of the EMT. Several studies were reported that CD133 expression contributes to tumor survival under hypoxia. Soeda et al. [53] showed that hypoxia could promote $CD133^{+}$ cancer stem-like cells expansion by upregulating HIF-1α. Furthermore, Hashimoto et al. [54] also found that hypoxia could encourage CD133 expression with HIF-1α. However, the mechanism of an interaction between CD133 and HIF-1α is still unclear. In the present study, we showed the possibility that CD133 does not affects HIF-1α expression as well as vimentin. These findings are at odds with the hypothesis that EMT is necessary to sustain the CSC phenotype, and they imply that the expression between CD133 and CD44 markers have uncoupled each other and CD133 expression does not connect with EMT in each of the substrate conditions tested in this study.

Taken together, CSC phenotype may not be rigid. Rather, interconversion of CSCs and non-CSCs might be a relatively common phenomenon that is driven by environmental stimuli (tanδ feature), or simply by stochasticity.

Previous reports showed that high CD133 expression is especially correlated with tumorigenicity, metastasis, and worse prognosis [26,27]. It has a strong potential as a target for drug therapies, since many breast cancer cell lines will express this marker. Indeed, it is still a matter of debate whether $CD133^{+}$cells truly represent the ultimate tumorigenic population. However, the belief that CD133 may act as a universal marker of CSCs has been met with a high degree of controversy in the research community. On the basis of the involvement of CSCs in tumorigenesis and treatment resistance, it is conceivable that only eradication of CSCs can lead to a cancer cure.

Conclusions

For CD133 and CD44 expression of MCF-7 cells, the expression of $CD133^{-}CD44^{+}$ is uncoupled from that of $CD133^{+}CD44^{-}$ in MCF-7 cells under different oxygen concentration levels. The $CD133^{-}CD44^{+}$ levels were promoted by damping coefficient, suggesting the softer gel substrate produce a large amount of surface molecule of CD44. For the co-expression of $CD133^{+}CD44^{+}$, seemed to be affected by the combination of both $CD133^{+}CD44^{-}$ and $CD133^{-}CD44^{+}$.

EMT was more promoted in both normoxic and hypoxic environment when MCF-7 cells incubated on softer gel substrate, especially on AC-soft (tanδ of 0.244) substrate, as revealed by EMT marker genes analysis. A significant association between $CD133^{-}CD44^{+}$ levels and vimentin/CDH2 expression in the cells incubated on AC-soft substrate under normoxia and hypoxia was observed, indicating the cells on softer substrate have a survival advantage due to the EMT. In contrast, for the $CD133^{+}CD44^{-}$ levels, their tanδ-dependent manner was not contributed by EMT phenomenon and was an independent from acquisition of the EMT.

The substrate damping as potential physical parameter emerged the important linkage to cellular motility, cancer stemness, and EMT induction. Although further investigation is required to clarify the efficacy of environmental stimuli (tanδ feature) for tumors exhibiting CSC-like properties, our study indicates that the MCF-7 cells incubated on softer substrate might lead to express CSC biomarkers exhibiting high CD44 and CD133 expression.

Acknowledgements

This work was supported by the TTI Grant (Special Research Project: FY2019-2020).

Competing Interests

The authors have declared that no competing interests exist.

References

1. Health, Labour and Welfare Ministry, Japan. Available at: http://www.mhlw.go.jp/toukei/saikin/hw/jinkou/geppo/nengai19/dl/h7.pdf [Accessed 16 November 2020].
2. Cancer morbidity and mortality. Available at: https://ganjoho.jp/reg_stat/statistics/stat/short _pred.html [Accessed 16 November 2020]
3. Allemani C, Weir HK, Carreira H, Harewood R, Spika D, et al. (2015) Global surveillance of cancer survival 1995–2009: analysis of individual data for 25 676 887 patients from 279 population-based registries in 67 countries (CONCORD-2). Lancet 385: 977-1010.
4. Hanahan D, Weinberg RA (2011) Hallmarks of Cancer: The Next Generation. Cell 144: 646-674.
5. De Craene B, Berx G (2013) Regulatory networks defining EMT during cancer initiation and progression. Nat Rev Cancer 13: 97-110.
6. Gil J, Stembalska A, Pesz KA, Sasjadek MM (2008) Cancer stem cells: the theory and perspectives in cancer therapy. J App Genet 49: 193-199.
7. McAllister SS, Weinberg RA (2014) The tumour-induced systemic environment as a critical regulator of cancer progression and metastasis. Nat Cell Biol 16: 717-727.
8. Taddei ML, Giannoni E, Comito G, Chiarugi P (2013) Microenvironment and tumor cell plasticity: An easy way out. Cancer lett 341: 80-96.
9. Giordano A, Gao H, Anfossi S, Cohen E, Mego M, et al. (2012) Epithelial-mesenchymal transition and stemcellmarkers in patients with HER2-positivemetastatic breast cancer. Mol Cancer Ther 11: 2526-2534.
10. Yip AK, Iwasaki K, Ursekar C, Machiyama H, Saxena M, et al. (2013) Cellular response to substrate rigidity is governed by either stress or strain. Biophys J 104: 19-29.
11. Ishikawa Y, Sasaki R, Domura R, Okamoto M (2019) Cellular morphologies, motility, and epithelial-mesenchymal transition of breast cancer cells incubated on viscoelastic gel substrates in hypoxia. Mater Today Chem 13: 8-17.
12. Jiang F, Khairy K, Poole K, Howard J, Müller DJ (2004) Creating nanoscopic collagen matrices using atomic force microscopy. Microsc Res Tech 64: 435-440.
13. Helmuth JA, Burckhardt CJ, Greber UF, Sbalzarini IF (2009) Shape reconstruction of subcellular structures from live cell fluorescence microscopy images. J Struct Biol 167: 1-10.
14. Tranquillo RT, Lauffenburger DA, Zigmond SH (1988) A stochastic model for leukocyte random motility and chemotaxis based on receptor binding fluctuations. J Cell Biol 106: 303-309.
15. Tzvetkova-Chevolleau T, Stephanou A, Fuard D, Ohayon J, Schiavone P, et al. (2008) The motility of normal and cancer cells in response to the combined influence of the substrate rigidity and anisotropic microstructure. Biomaterials 29: 1541-1551.
16. Wang YC, Ludwigson M, Lakes RS (2004) Deformation of extreme viscoelastic metals and composites. Mater Sci Eng A 370: 41-49.
17. Butcher DT, Alliston T, Weaver VM (2009) A tense situation: forcing tumour progression. Nat Rev Cancer 9: 108-122.

18. Ishihara S, Yasuda M, Harada I, Mizutani T, Kawabata K, et al. (2013) Substrate stiffness regulates temporary NF-κB activation via actomyosin contractions. Exp Cell Res 319: 2916-2927.
19. Dalby MJ, Gadegaard N, Tare R, Andar A, Riehle MO, et al. (2007) The control of human mesenchymal cell differentiation using nanoscale symmetry and disorder. Nat Mater 6: 997-1003.
20. Chaudhuri PK, Pan CQ, Low BC, Lim CT (2016) Topography induces differential sensitivity on cancer cell proliferation via Rho-ROCK-Myosin contractility. Sci Rep 6: 19672.
21. Wu J, Chu C-C (2012) Block copolymer of poly (ester amide) and polyesters: Synthesis, characterization, and *in vitro* cellular response. Acta Biomater 8: 4314-4323.
22. Mih JD, Marinkovic A, Liu F, Sharif AS, Tschumperlin DJ (2012) Matrix stiffness reverses the effect of actomyosin tension on cell proliferation. J Cell Sci 125: 5974-5983.
23. O'brien CA, Pollett A, Gallinger S, Dick JE (2007) A human colon cancer cell capable of initiating tumour growth in immunodeficient mice. Nature 445: 106-110.
24. Yang D, Wang H, Zhang J, Li C, Lu Z, et al. (2013) *In vitro* characterization of stem cell-like properties of drug-resistant colon cancer subline. Oncol Res 21: 51-57.
25. Matsuda Y, Kure S, Ishiwata T (2012) Nestin and other putative cancer stem cell markers in pancreatic cancer. Med Mol Morphol 45: 59-65.
26. Chen S, Song X, Chen Z, Li X, Li M, et al. (2013) CD133 expression and the prognosis of colorectal cancer: a systematic review and meta-analysis. PLoS ONE 8: e56380.
27. Sahlberg SH, Spiegelberg D, Glimelius B, Stenerlöw B, Nestor M (2014) Evaluation of cancer stem cell markers CD133, CD44, CD24: association with AKT isoforms and radiation resistance in colon cancer cells. PLoS ONE 9: e94621.
28. Schneider M, Huber J, Hadaschik B, Siegers GM, Heinz-Herbert F, et al. (2012) Characterization of colon cancer cells: a functional approach characterizing CD133 as a potential stem cell marker. BMC Cancer 12: 96.
29. Xie J, Xiao Y, Zhu X-Y, Ning Z-Y, Xu H-F (2016) Hypoxia regulates stemness of breast cancer MDA-MB-231 cells. Med Oncol 33: 42.
30. Yilmaz M, Christofori G (2009) EMT, the cytoskeleton, and cancer cell invasion. Cancer Metastasis Rev 28: 15-33.
31. Nieman MT, Prudoff RS, Johnson KR, Wheelock MJ (1999) N-Cadherin Promotes Motility in Human Breast Cancer Cells Regardless of their E-Cadherin Expression. J Cell Biol 147: 631-643.
32. Hulit J, Suyama K, Chung S, Keren R, Agiostratidou G, et al. (2007) N-cadherin signaling potentiates mammary tumor metastasis via enhanced extracellular signal-regulated kinase activation. Cancer Res 67: 3106-3116.
33. Vuoriluoto K, Haugen H, Kiviluoto S, Mpindi J, Nevo J, et al. (2011) Vimentin regulates EMT induction by Slug and oncogenic H-Ras and migration by governing Axl expression in breast cancer. Oncogene 30: 1436-1448.
34. Satelli A, Li S (2011) Vimentin as a potential molecular target in cancer therapy Or Vimentin, an overview and its potential as a molecular target for cancer therapy. Cell Mol Life Sci 68: 3033-3046.
35. Tam WL, Weinberg RA (2013) The epigenetics of epithelial-mesenchymal plasticity in cancer. Nat Med 19: 1438-1439.
36. Polyak K, Weinberg RA (2009) Transitions between epithelial and mesenchymal states: acquisition of malignant and stem cell traits. Nat Rev Cancer 9: 265-273.
37. Thiery JP (2002) Epithelial–mesenchymal transitions in tumour progression. Nat Rev Cancer 2: 442-454.

38. Iwatsuki M, Mimori K, Yokobori T, Ishi H, Beppu T, et al. (2010) Epithelial–mesenchymal transition in cancer development and its clinical significance. Cancer Sci 101: 293-299.
39. Olmeda D, Moreno-Bueno G, Flores JM, Fabra A, Portillo F, et al. (2007) SNAI1 is required for tumor growth and lymph node metastasis of human breast carcinoma MDA-MB-231 cells. Cancer Res 67: 11721-11731.
40. Nasrollahi S, Pathak A (2016) Topographic confinement of epithelial clusters induces epithelial-to-mesenchymal transition in compliant matrices. Sci Rep 6: 18831.
41. Zavadil J, Böttinger EP (2005) TGF-beta and epithelial-to-mesenchymal transitions. Oncogene 24: 5764-5774.
42. Janda E, Evolo M, Lehmann K, Downward J, Beug H, et al. (2006) Grieco M. Raf plus TGFB-dependent EMT is initiated by endocytosis and lysosomal degradation of E-cadherin. Oncogene 25: 7117-7130.
43. Peinado H, Olmeda D, Cano A (2007) Snail, Zeb and bHLH factors in tumour progression: an alliance against the epithelial phenotype? Nat Rev Cancer 7: 415-428.
44. Wei SC, Fattet L, Tsai JH, Guo Y, Pai VH, et al. (2015) Matrix stiffness drives epithelial–mesenchymal transition and tumour metastasis through a TWIST1–G3BP2 mechanotransduction pathway. Nat Cell Biol 17: 678-688.
45. Gregory PA, Bert AG, Paterson EL, Barry SC, Tsykin A, et al. (2008) The miR-200 family and miR-205 regulate epithelial to mesenchymal transition by targeting ZEB1 and SIP1. Nat Cell Biol 10: 593-601.
46. Eger A, Aigner K, Sonderegger S, Dampier B, Oehler S, et al. (2005) Schreiber M, Berx G, Cano A, Beug H, Foisner R. DeltaEF1 is a transcriptional repressor of E-cadherin and regulates epithelial plasticity in breast cancer cells. Oncogene 24: 2375-2385.
47. Gilkes DM, Bajpai S, Chaturvedi P, Wirtz D, Semenza GL (2013) Hypoxia-inducible factor 1 (HIF-1) promotes extracellular matrix remodeling under hypoxic conditions by inducing P4HA1, P4HA2, and PLOD2 expression in fibroblasts. J Biol Chem 288: 10819-10829.
48. Gilkes DM, Xiang L, Lee SJ, Chaturvedi P, Hubbi ME, et al. (2014) Hypoxia-inducible factors mediate coordinated RhoA-ROCK1 expression and signaling in breast cancer cells. Proc Natl Acad Sci USA 111: E284-E393.
49. Schito L, Semenza GL (2016) Hypoxia-Inducible Factors: Master Regulators of Cancer Progression. Trends Cancer 2: 758-770.
50. Kreso A, Dick JE (2014) Evolution of the cancer stem cell model. Cell Stem Cell 14: 275-291.
51. Chaffer CL, Weinberg RA (2011) A perspective on cancer cell metastasis. Science 331: 1559-1564.
52. Giancotti FG (2013) Mechanisms governing metastatic dormancy and reactivation. Cell 155: 750-764.
53. Soeda A, Park M, Lee D, Mintz A, Androutsellis-Theotokis A, et al. (2009) Hypoxia promotes expansion of the CD133-positive glioma stem cells through activation of HIF-1α. Oncogene 28: 3949-3959.
54. Hashimoto O, Shimizu K, Semba S, Chiba S, Ku Y, et al. (2011) Hypoxia induces tumor aggressiveness and the expansion of CD133-positive cells in a hypoxia-inducible factor-1α-dependent manner in pancreatic cancer cells. Pathobiology 78: 181-192.